Multiscale Microrheology Using Fluctuating Filaments as Stealth Probes

Kengo Nishi,[1,2,3] Fred C. MacKintosh,[4,5,6,7] and Christoph F. Schmidt[1,2]

[1]*Third Institute of Physics-Biophysics, Faculty of Physics, University of Göttingen, 37077 Göttingen, Germany*
[2]*Department of Physics & Soft Matter Center, Duke University, Durham, North Carolina 27708, USA*
[3]*Department of Applied Physical Sciences, University of North Carolina, Chapel Hill, North Carolina 27599, USA*
[4]*Department of Chemical & Biomolecular Engineering, Rice University, Houston, Texas 77005, USA*
[5]*Center for Theoretical Biological Physics, Rice University, Houston, Texas 77030, USA*
[6]*Department of Chemistry, Rice University, Houston, Texas 77005, USA*
[7]*Department of Physics & Astronomy, Rice University, Houston, Texas 77005, USA*

The mechanical properties of soft materials can be probed on small length scales by microrheology. A common approach tracks fluctuations of micrometer-sized beads embedded in the medium to be characterized. This approach yields results that depend on probe size when the medium has structure on comparable length scales. Here, we introduce filament-based microrheology using high-aspect-ratio semiflexible filaments as probes. Such quasi-1D probes are much less invasive than beads due to their small cross sections. Moreover, by imaging transverse bending modes, we simultaneously determine the micromechanical response of the medium on multiple length scales corresponding to the mode wavelengths. We use semiflexible single-walled carbon nanotubes as probes that can be accurately and rapidly imaged based on their stable near-IR fluorescence. We find that the viscoelastic properties of sucrose, polyethylene oxide, and hyaluronic acid solutions measured in this way are in good agreement with those measured by conventional micro- and macrorheology.

Soft materials such as polymer solutions display structure at many scales and exhibit relaxation times from ms to > hrs. Conventional macroscopic rheology is mostly appropriate for time scales $\gtrsim 0.1$ s [1], and for samples with shear elastic moduli $\gtrsim 1$ Pa [2]. Various microrheology (MR) techniques have been developed to probe soft materials in the μs to s range, using μm-sized particles [3–7]. Small probes also allow one to study small samples in confined geometries. MR is sensitive to length scales $\gtrsim$ probe size [8–10]. While simple continuum mechanics might not always be appropriate to interpret data, MR can be used to explicitly probe local structure in complex media. Correlated fluctuations of pairs of particles can be monitored to probe response on varying length scales (particle distance) [5,11,12]. Probes can create artifacts, and particular samples might not be accessible to the probes. This holds for biological cells or tissues, where beads are even actively expelled from, e.g., the cell nucleus, the mitotic spindle, or the actin cortex [13–16].

Here, we introduce the use of slender filaments, semiflexible polymers, as local *stealth probes*. Filaments embedded in a viscoelastic network, such as microtubules in the cell cytoskeleton [17,18], undulate with the motions of the network, but their bending stiffness also affects network fluctuations. While the filament length is relevant for the hydrodynamic interaction with the embedding medium, the filament diameter determines local perturbations due to excluded volume. We use minimally invasive single-walled carbon nanotubes (SWNTs) with extreme aspect ratios: diameters of ~ 1 nm and lengths up to tens of μm [Fig. 1(a)]. SWNTs have precisely known chemical structures and bending stiffnesses [19,20]. Semiconducting SWNTs exhibit photostable near-IR fluorescence, permitting long-time, high-resolution tracking of their positions and shapes [20]. We decompose shapes into dynamic bending eigenmodes [Fig. 1(b)]. Each mode is sensitive to the medium properties on the scale of its wavelength, similar to membranes [21–25]. By resolving bending modes with wavelengths up to tens of μm, we simultaneously measure medium response on multiple length scales using a single filament. Filament microrheology (FMR) offers advantages over conventional MR: (1) multiple length scales can be probed simultaneously; (2) the mechanical sensitivity can be varied by varying filament stiffness; and (3) the method can even use endogenous cytoskeletal biopolymers, such as actin filaments and microtubules.

We parameterize the shape of a weakly undulating filament at time t by the transverse deflection $u(s, t)$ along its arc length s. We describe transverse filament motion by a generalized Langevin equation describing the net force per unit length on the chain at position s [26,27]:

$$0 = -\kappa \frac{\partial^4}{\partial s^4} u(s, t) - \int_{-\infty}^{t} dt' \alpha(t - t') u(s, t') + \xi(s, t). \quad (1)$$
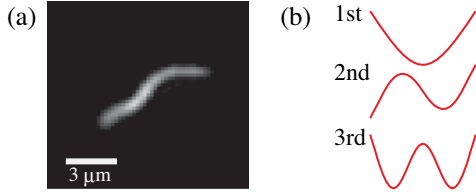
FIG. 1.   (a) A near-infrared fluorescence image of a SWNT in a 4.5 mg/ml hyaluronic acid solution. (b) The first three spatial dynamic eigenmodes of an elastic beam with free ends.

The first term accounts for the elastic restoring force [27], with bending rigidity κ. The second term is the viscoelastic drag, where the resistance per unit length is given by the memory function $\alpha(t)$, whose Fourier transform $\alpha(\omega)$ is proportional to the complex shear modulus of the medium, $G(\omega)$ [28,29]. For the transverse displacement of a rigid rod of length L and diameter d in a viscous liquid, $\alpha(\omega) \simeq -4\pi i \omega \eta / \ln(AL/d)$, where $A \simeq 2.3$, and η is the viscosity [30–33]. The Brownian force $\xi(s,t)$ has a zero mean $\langle \xi(s,t) \rangle = 0$ and a power spectrum satisfying $\langle \xi(s,\omega)\xi(s',\omega) \rangle = (2k_B T/\omega)\delta(s-s')\text{Im}[\alpha(\omega)]$, with Boltzmann's constant k_B and temperature T, as required by the fluctuation dissipation theorem (FDT).

We expand $u(s,t)$ into orthogonal dynamic eigenmodes $y_q(s)$ as $u(s,t) = \sum_q a_q(t)y_q(s)$ with wave number $q = \alpha_k/L = (k + \frac{1}{2})\pi/L$ for free-end boundary conditions [26] (see Supplemental Material [34]). The projection of Eq. (1) onto a particular spatial mode $y_q(s)$ gives the equation of motion $0 = -\int_{-\infty}^t dt' \alpha(t-t')a_q(t') - \kappa q^4 a_q(t) + \xi_q(t)$. Assuming linear response to the Fourier component of the force f_q, the mode amplitude will be $a_q(\omega) = \chi_q(\omega)f_q(\omega)$, with the response function $\chi_q(\omega) = (\kappa q^4 + \alpha(\omega))^{-1}$. The FDT relates the amplitude autocorrelation function $C_q(t) = \langle a_q(t)a_q(0) \rangle$ of each mode k to the corresponding time-dependent response function $\chi_q(t)$ for $t > 0$: [38,39]

$$k_B T \chi_q(t) = -\frac{d}{dt}\langle a_q(t)a_q(0) \rangle = \frac{1}{2}\frac{d}{dt}M_q(t), \quad (2)$$

where the mean-squared amplitude difference (MSAD) is defined as $M_q(t) = \langle [a_q(t) - a_q(0)]^2 \rangle = \langle [\Delta a_q(t)]^2 \rangle$. Fourier transformation gives the frequency-dependent response function $\chi_q(\omega) = \chi_q'(\omega) + i\chi_q''(\omega) = \int_0^\infty dt \chi_q(t)e^{i\omega t}$. We applied the five-point stencil method to accurately calculate the numerical derivative and Simpson's rule for the subsequent integral [39]. The response function $\chi_q(\omega)$ is thus calculated from direct integral transforms of the MSAD using the FDT. Alternatively, $\chi_q(\omega)$ and $G(\omega)$ can be derived from the bending fluctuations using a Kramers-Kronig integral (KK integral) [4] (Fig. S11). In order to avoid bias, we do not use functional fitting [3] or interpolation [40,41]. The complex functions $\alpha(\omega)$ and $G(\omega)$ can be evaluated from $\chi_q(\omega)$ via

$$\chi_q(\omega)^{-1} - \kappa q^4 = \alpha(\omega) \simeq 4\pi G(\omega)/\ln(AL_{\text{eff}}/d), \quad (3)$$

where $L_{\text{eff}} \simeq L/(k + \frac{1}{2})$ is the characteristic length of the undulation [29]. For a SWNT diameter of ~ 1 nm and L_{eff} of ~ 3 μm, $\alpha \simeq 1.4G(\omega)$.

We assume small undulations, i.e., slope $|du/ds| \ll 1$ and mode amplitudes $|qa_q| \ll 1$ (Fig. S3). Equation (3) shows that for high q, the energy is dominated by bending and becomes insensitive to the modulus of the surrounding medium (Fig. S3). This limits the bending stiffness that can be used to probe a specific material. Conversely, this also permits to adapt the technique for diverse soft materials, largely independent of the length scale probed. By contrast, the mechanical sensitivity and the characteristic length scale probed with particle-based MR is determined by just one parameter, the particle size.

We tested our method on three materials: a viscoelastic hyaluronic acid (HA) ($M_w = 2 - 2.4$ MDa) solution, a purely viscous sucrose solution, and a polyethylene oxide (PEO) solution ($M_v \sim 8$ MDa) as a well-established standard. Surfactant-wrapped SWNTs were mixed into these solutions and illuminated with a 561 nm laser (see Supplemental Material [34]). This wavelength resonantly excited SWNTs of (6,5) chirality and 0.78 nm diameter [20,42,43].

HA is an anionic glycosaminoglycan with nontrivial viscoelasticity prevalent in the pericellular matrix of cells [44]. Figure 2(a) shows bending mode dynamics of a ~ 5 μm long SWNT in a 3 mg/ml HA solution. Mode amplitudes fluctuated around 0 (intrinsically straight filaments) and decreased for the higher modes as expected for thermal modes. Figure 2(b) shows MSADs for modes 1 to 3. The bending fluctuations of SWNTs exceeded noise for the first three modes (Fig. S2). At times < 1 s, all MSADs exhibit a power law slope < 1, reflecting the viscoelasticity of the system [Fig. 2(b)]. At long times, MSADs reach a plateau because filament bending modulus dominates over medium response. Note that this is also observed in a purely viscous medium. MSADs of higher modes reach the plateau earlier due to the higher bending energy for a given amplitude. From equipartition, the total variance of mode amplitude fluctuations $\langle a_q(0)^2 \rangle$ should be inversely proportional to bending rigidity and scale with wave number as [27,33] $\langle a_q(0)^2 \rangle = k_B T/\kappa q^4$. This prediction is plotted in the inset of Fig. 2(b), matching our data using $\kappa = 1.26 \times 10^{-25}$ J m from Ref. [20] (this value used for further analysis).

Thermal SWNT fluctuations and tracking results in a 4.5 mg/ml HA solution are shown in Fig. S6. It is important to take into account that the higher modes of shorter SWNTs are not suitable to measure $G'(\omega)$ because $\kappa q^4/k_0 \gg G'(\omega)$ (Fig. S3). Since the low-frequency $G'(\omega)$ was ~ 0.1 Pa, we chose mode numbers that fulfill $\kappa q^4/k_0 \lesssim 0.1$ Pa with $q = (k + 1/2)\pi/L$ to estimate $G'(\omega)$. Complex shear moduli calculated from different modes agree as expected since HA response is not scale dependent
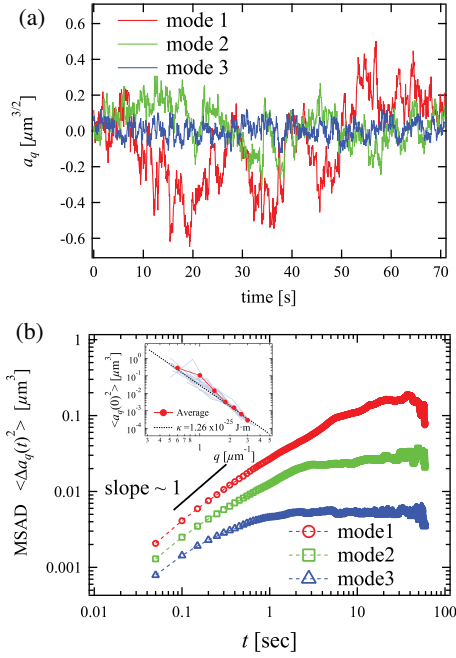
FIG. 2. (a) Amplitudes of modes 1 to 3 of a 5 μm SWNT in a 3 mg/ml HA solution. (b) MSADs for the same modes (5 recordings). Inset: variance of mode amplitudes plotted vs wave number (18 recordings from five SWNTs in the same solution, lengths $4.5 \sim 8.5$ μm) black (blue lines). Averages smoothed by binning (red circles). Expected dependence $\langle a_q(0)^2 \rangle = k_B T / \kappa q^4$ with $\kappa = 1.26 \times 10^{-25}$ J $\cdot$ m [20] (black dashed line).

in the μm range. Filament and bead MR show good agreement [Fig. 3(a), Fig. S7, and Fig. S8]. G_{fil} calculated from the first bending mode and G_{bead} agree and scale with concentration from 1 to 4.5 mg/ml (Fig. S8), confirming that FMR sensitively captures the concentration dependence of the viscoelasticity of HA solutions. At high frequencies, G_{bead} extends beyond G_{fil} because of different recording frame rates: 50 Hz for bead MR and 10/20 Hz for FMR. To demonstrate consistency, real and imaginary parts of G_{bead} were fitted by power laws, and both components of G_{fil} derived from multiple bending modes were normalized by the bead results (Fig. S10).

Complex shear moduli increase with increasing HA concentration as expected [Fig. 3(a), Fig. S7, and Fig. S8]. To analyze the frequency dependence at different polymer concentrations, we fitted G''_{bead} with power laws [Fig. 3(a), Fig. S7]. For 1 mg/ml HA the slope is close to 1, reflecting purely viscous response. The slope decreases with increasing HA concentration, reflecting increasing viscoelastic response, consistent with previous studies [44]. We did not observe a plateau, even in the 4.5 mg/ml HA solution, implying at most weak entanglement. This is expected since the overlap concentration c^* for the HA we used is ~0.3 mg/ml. An elastic plateau is expected only at around 10 mg/ml [44].

Figure 3(a) also shows data obtained from a single 19 μm long SWNT in the 4.5 mg/ml HA solution. We could evaluate 8 modes. For modes 1–4, the recording time was too short to allow full equilibration (see Supplemental Material and Fig. S12 [34]). G_{fil} calculated from modes 5–8 is consistent with G_{bead}. The effective length of mode 8 ($L_{eff} = 2.2$ μm) is 5.7 times shorter than that of mode 1 ($L_{eff} = 12.7$ μm), illustrating the unique possibility to simultaneously measure medium response over a range of length scales with a single filament.

We next quantitatively confirmed FMR in a 60 wt% sucrose solution, a Newtonian fluid. We analyzed 24 movies of 8 fluctuating SWNTs with lengths of 4.5–6 μm. Resulting complex shear moduli are shown in Fig. S5. As expected for a Newtonian fluid, the values of $G''(\omega)$ from both modes collapse onto a single curve with a power-law slope of ~1, while $G'(\omega)$ from the first mode fluctuates around 0. $G''(\omega)$ of this solution obtained by macroscopic rheology with parallel-plate geometry agrees well (Fig. S5).

To further confirm FMR in a standard viscoelastic material, we studied a semidilute solution of high-molecular-weight polyethylene oxide (PEO). We again chose the appropriate mode numbers, such that $\kappa q^4 / k_0 \lesssim 0.1$ Pa to estimate $G'(\omega)$. Results from filament bending dynamics (G_{fil}) agree with those obtained from bead MR (G_{bead}) and bulk rheology [Fig. 3(b)]. Note that bulk rheology may not give reliable results for soft materials with moduli below ~1 Pa (Fig. S9). Therefore, we here consider the comparison of our new FMR method with an established MR method as most relevant.

FMR can also be used to characterize the fluctuating filaments. Equation (3) shows that filament dynamics depend on medium response and filament bending stiffness. When bending stiffness is known, FMR can measure medium response. Alternatively, we can obtain filament stiffness if medium response is known. To demonstrate this, we performed a global 2D fit of power spectral densities (PSDs) $\langle |a_q(\omega)|^2 \rangle$ of mode amplitude time series from several filaments. The PSD is the Fourier transform of the MSAD. The scale-dependent PSDs plotted in Fig. 3(c) can be described starting from the generalized Langevin equation, Eq. (1). With the PSD of the Brownian force: $\langle \xi(s,\omega)\xi(s',\omega) \rangle = (2k_B T/\omega)\delta(s-s')\text{Im}[\alpha(\omega)]$, we find: $\langle |a_q(\omega)|^2 \rangle = (k_B T/\omega)\text{Im}[\chi_q(\omega)] = (k_B T/\omega)[\alpha''(\omega)/|\kappa q^4 + \alpha(\omega)|^2]$ (4) with $q = (k+1/2)\pi/L$ for mode number k. We can thus globally fit all the scale-dependent PSDs with a single 2D plane defined by Eq. (4), with just one free parameter, κ, having fixed the memory function $\alpha(\omega) = k_0 G(\omega)$ with the power-law fitting results of G_{bead} [Fig. 3(c)]. We used modes 1,2,3 of three SWNTs with lengths of 9.15, 6.13, and 5.03 μm in 3 mg/ml HA to obtain SWNT bending stiffness. At low frequencies, PSDs level off for the higher q modes when the filament bending modulus restricts thermal bending amplitudes. Slices through the fitted plane at the respective q values

(a) HA solution
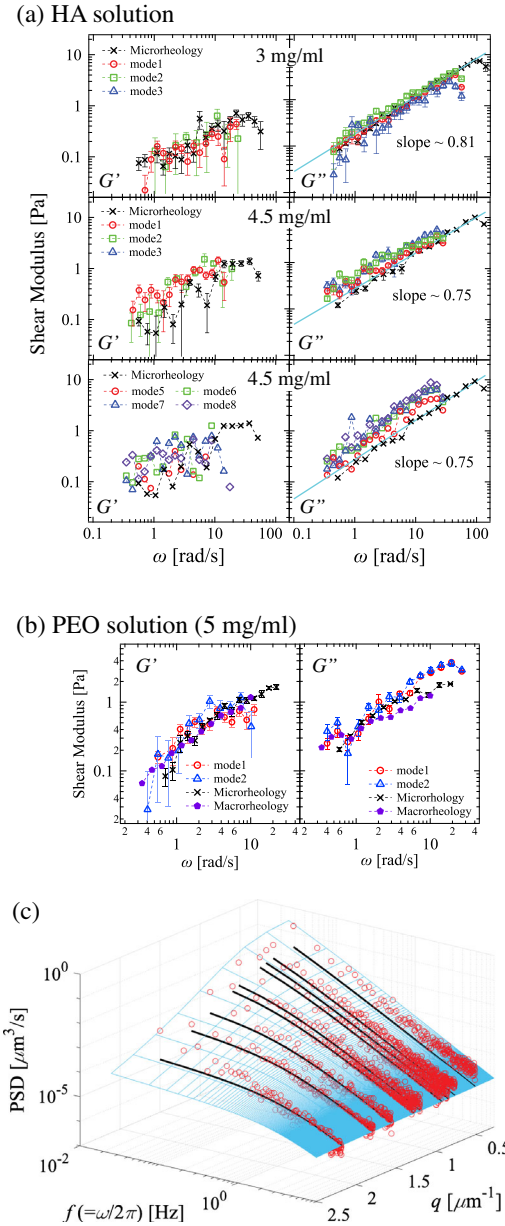
(b) PEO solution (5 mg/ml)

(c)

FIG. 3. (a) Viscoelasticity of HA solutions measured from the bending dynamics of SWNTs. HA concentrations given in graphs. Upper row: 18 recordings from 5 SWNTs, lengths $4.5 \sim 8.5 \ \mu m$. Middle row: 14 recordings from 8 SWNTs, lengths $4.5 \sim 7.5 \ \mu m$. Bottom row: 1 SWNT, length 19 μm. Shear elastic moduli of each HA solution were also measured by conventional bead MR (black crosses). Power-law fits of G''_{bead} MR are shown as solid light blue lines. (b) Viscoelasticity of a 5 mg/ml 8 MDa PEO solution measured from the bending dynamics of SWNTs (20 recordings from three SWNTs averaged). (c) Global 2D fit of PSDs as a function of wave number q and frequency $f (= \omega/2\pi)$ (10 recordings from three SWNTs with lengths of 9.15, 6.13, and 5.03 μm). Three modes (1 to 3) of each SWNT are plotted. The fit with Eq. (4) is shown as light-blue mesh plane. Black solid lines represent slices of the fitted plane at $q = 0.515, 0.769, 0.858, 0.937, 1.20, 1.28, 1.56, 1.79,$ and $2.19 \ \mu m^{-1}$, which correspond to the wave numbers of three modes (1 to 3) of SWNTs with lengths of 9.15, 6.13, and 5.03 μm, respectively.

can be compared with the data. From this fit, we find $\kappa = (7.09 \pm 1.04) \times 10^{-26}$ J m, close to the reported value $\kappa = 1.26 \times 10^{-25}$ J m [20].

Thermal bends of a filament in a polymer network can relax either by following the relaxation of the surrounding network or by reptation, i.e., anisotropic diffusion through the network [45–50]. Reptation contributes to mode-amplitude relaxation if it occurs rapidly enough to compete with network dynamics [47,51]. We neglect reptation here since in the viscous or weakly elastic solutions we probed, medium relaxation was dominant. In more strongly entangled polymer networks, reptation needs to be taken into account or suppressed by crosslinking the probe filament to the network. Shorter-wavelength modes should be less affected by reptation artifacts than longer-wavelength modes. In our data, moduli calculated from different modes coincide, and the results also coincide with those from conventional micro- and macrorheology, proving that reptation was indeed negligible here.

To quantify the stealth character of FMR we can estimate how local depletion and nonaffine deformations around the probe [13–16], affect results. Probe geometry enters through Eq. (3) in the relation $\alpha(\omega) = k_0 G(\omega)$ with, $k_0 \approx 4\pi/\ln(AL_{eff}/d)$ for a filament. For a SWNT with 0.78 nm diameter and 10 μm length, the error of the shape factor k_0 would be less than 8% even if the effective diameter of the filament were to double due to local nonaffine deformations. Because k_0 is inversely proportional to the logarithm of its aspect ratio, FMR is thus quite insensitive to local perturbations due to the filament cross section.

In conclusion, we have introduced and tested filament microrheology (FMR), evaluating the bending dynamics of embedded filaments as a new method to measure shear elastic moduli in soft viscoelastic media. Slender filaments with two dimensions on the nm scale and lengths on the μm scale cause minimal local perturbations, easily penetrate dense media such as cell-internal structures or the nucleus, while still coupling to mesoscopic medium dynamics on the μm scale. Furthermore, filaments report complex shear moduli at multiple length scales simultaneously. FMR is thus uniquely useful to measure the scale-dependent viscoelasticity of soft materials with hierarchical structures, for example the cytoskeleton of living cells. In our samples we found good agreement with conventional MR over almost 2 orders of magnitude in frequency and with standard rheology. We expect that other semiflexible filaments such as actin filaments or microtubules can be used as probe filaments in biological systems, which would completely avoid the introduction of foreign objects into cells. Our approach also suggests possible extensions using the shape fluctuations of other extended objects such as membranes [21–25] to quantify the rheological properties of the surrounding medium.

[1] C. W. Macosko and I. M. Krieger, *Rheology: Principles, Measurements, and Applications* (Wiley-VCH, New York, 1996), Vol. 178.

[2] *Complex Fluids in Biological Systems*, edited by E. S. Spagnolie (Springer, New York, 2014).

[3] T. G. Mason and D. A. Weitz, Phys. Rev. Lett. 74, 1250 (1995).

[4] F. Gittes, B. Schnurr, P. D. Olmsted, F. C. MacKintosh, and C. F. Schmidt, Phys. Rev. Lett. 79, 3286 (1997).

[5] J. C. Crocker, M. T. Valentine, E. R. Weeks, T. Gisler, P. D. Kaplan, A. G. Yodh, and D. A. Weitz, Phys. Rev. Lett. 85, 888 (2000).

[6] F. C. MacKintosh and C. F. Schmidt, Curr. Opin. Colloid Interface Sci. 4, 300 (1999).

[7] E. M. Furst and T. M. Squires, *Microrheology* (Oxford University Press, New York, 2017).

[8] A. W. C. Lau, B. D. Hoffman, A. Davies, J. C. Crocker, and T. C. Lubensky, Phys. Rev. Lett. 91, 198101 (2003).

[9] D. Mizuno, C. Tardin, C. F. Schmidt, and F. C. MacKintosh, Science 315, 370 (2007).

[10] M. Guo, A. J. Ehrlicher, M. H. Jensen, M. Renz, J. R. Moore, R. D. Goldman, J. Lippincott-Schwartz, F. C. MacKintosh, and D. A. Weitz, Cell 158, 822 (2014).

[11] L. A. Hough and H. D. Ou-Yang, Phys. Rev. E 65, 021906 (2002).

[12] M. Buchanan, M. Atakhorrami, J. F. Palierne, F. C. MacKintosh, and C. F. Schmidt, Phys. Rev. E 72, 011504 (2005).

[13] D. T. Chen, E. R. Weeks, J. C. Crocker, M. F. Islam, R. Verma, J. Gruber, A. J. Levine, T. C. Lubensky, and A. G. Yodh, Phys. Rev. Lett. 90, 108301 (2003).

[14] M. T. Valentine, Z. E. Perlman, M. L. Gardel, J. H. Shin, P. Matsudaira, T. J. Mitchison, and D. A. Weitz, Biophys. J. 86, 4004 (2004).

[15] J. He and J. X. Tang, Phys. Rev. E 83, 041902 (2011).

[16] M. Atakhorrami, G. H. Koenderink, J. F. Palierne, F. C. MacKintosh, and C. F. Schmidt, Phys. Rev. Lett. 112, 088101 (2014).

[17] C. P. Brangwynne, F. C. MacKintosh, and D. A. Weitz, Proc. Natl. Acad. Sci. U.S.A. 104, 16128 (2007).

[18] C. P. Brangwynne, G. H. Koenderink, F. C. MacKintosh, and D. A. Weitz, Phys. Rev. Lett. 100, 118104 (2008).

[19] K. N. Kudin, G. E. Scuseria, and B. I. Yakobson, Phys. Rev. B 64, 235406 (2001).

[20] N. Fakhri, D. A. Tsyboulski, L. Cognet, R. B. Weisman, and M. Pasquali, Proc. Natl. Acad. Sci. U.S.A. 106, 14219 (2009).

[21] F. Brochard and J. F. Lennon, J. Phys. (Paris), Lett. 36, 1035 (1975).

[22] E. Helfer, S. Harlepp, L. Bourdieu, J. Robert, F. C. MacKintosh, and D. Chatenay, Phys. Rev. E 63, 021904 (2001).

[23] E. Helfer, S. Harlepp, L. Bourdieu, J. Robert, F. C. MacKintosh, and D. Chatenay, Phys. Rev. Lett. 87, 088103 (2001).

[24] A. J. Levine and F. C. MacKintosh, Phys. Rev. E 66, 061606 (2002).

[25] R. Granek, Soft Matter 7, 5281 (2011).

[26] S. R. Aragon and R. Pecora, Macromolecules 18, 1868 (1985).

[27] F. Gittes, B. Mickey, J. Nettleton, and J. Howard, J. Cell Biol. 120, 923 (1993).

[28] L. D. Landau and E. M. Lifshitz, *Theory of Elasticity*, 3rd ed. (Pergamon Press, Oxford, England, 1986).

[29] C. P. Brangwynne, F. C. MacKintosh, S. Kumar, N. A. Geisse, J. Talbot, L. Mahadevan, K. K. Parker, D. E. Ingber, and D. A. Weitz, J. Cell Biol. 173, 733 (2006).

[30] R. G. Cox, J. Fluid Mech. 44, 791 (1970).

[31] S. Broersma, J. Chem. Phys. 74, 6989 (1981).

[32] G. Li and J. X. Tang, Phys. Rev. E 69, 061921 (2004).

[33] C. P. Brangwynne, G. H. Koenderink, E. Barry, Z. Dogic, F. C. MacKintosh, and D. A. Weitz, Biophys. J. 93, 346 (2007).

[34] See Supplemental Material at http://link.aps.org/supplemental/10.1103/PhysRevLett.127.158001 for further detail, which includes Refs. [35–37].

[35] M. Rubinstein and R. H. Colby, *Polymer Physics* (Oxford University Press, New York, 2003), Vol. 23.

[36] I. F. Sbalzarini and P. Koumoutsakos, J. Struct. Biol. 151, 182 (2005).

[37] M. B. Smith, H. Li, T. Shen, X. Huang, E. Yusuf, and D. Vavylonis, Cytoskeleton (Hoboken) 67, 693 (2010).

[38] D. Chandler, *Introduction to Modern Statistical Mechanics* (Oxford University Press, New York, 1987).

[39] K. Nishi, M. L. Kilfoil, C. F. Schmidt, and F. C. MacKintosh, Soft Matter 14, 3716 (2018).

[40] R. M. L. Evans, M. Tassieri, D. Auhl, and T. A. Waigh, Phys. Rev. E 80, 012501 (2009).

[41] M. Tassieri, R. M. L. Evans, R. L. Warren, N. J. Bailey, and J. M. Cooper, New J. Phys. 14, 115032 (2012).

[42] S. M. Bachilo, M. S. Strano, C. Kittrell, R. H. Hauge, R. E. Smalley, and R. B. Weisman, Science 298, 2361 (2002).

[43] D. A. Tsyboulski, S. M. Bachilo, and R. B. Weisman, Nano Lett. 5, 975 (2005).

[44] N. Nijenhuis, D. Mizuno, C. F. Schmidt, H. Vink, and J. A. E. Spaan, Biomacromolecules 9, 2390 (2008).

[45] S. F. Edwards, Proc. Phys. Math. Soc. Jpn. 92, 9 (1967).

[46] P.-G. de Gennes, J. Chem. Phys. 55, 572 (1971).

[47] M. Doi and S. F. Edwards, J. Chem. Soc., Faraday Trans. 2 74, 1789 (1978).

[48] J. Käs, H. Strey, and E. Sackmann, Nature (London) 368, 226 (1994).

[49] J. Käs, H. Strey, J. X. Tang, D. Finger, R. Ezzell, E. Sackmann, and P. A. Janmey, Biophys. J. 70, 609 (1996).

[50] N. Fakhri, F. C. MacKintosh, B. Lounis, L. Cognet, and M. Pasquali, Science 330, 1804 (2010).

[51] D. C. Morse, Macromolecules 31, 7044 (1998).